

# The van der Waals interaction as the starting point for an effective field theory

Daniel Odell,<sup>1,2,\*</sup> Arnoldas Deltuva,<sup>3</sup> and Lucas Platter<sup>1,4,†</sup>

<sup>1</sup>*Department of Physics and Astronomy,  
University of Tennessee, Knoxville, TN 37996, USA*

<sup>2</sup>*Department of Physics and Astronomy,  
Ohio University, Athens, OH 45701, USA*

<sup>3</sup>*Institute of Theoretical Physics and Astronomy,  
Vilnius University, Saulėtekio al. 3, LT-10257 Vilnius, Lithuania*

<sup>4</sup>*Physics Division, Oak Ridge National Laboratory, Oak Ridge, TN 37831, USA*

(Dated: May 11, 2021)

## Abstract

We consider the system of three  $^4\text{He}$  atoms to assess whether a pure van der Waals potential can be used as a starting point for an effective field theory to describe three-body processes in ultracold atomic systems. Using a long-range van der Waals interaction in combination with short-distance two-body counterterms, we analyze the dependence of two- and three-body observables on the short-distance regulator that is required due to the singular nature of the van der Waals interaction. We benchmark our approach with results obtained with the *realistic*  $^4\text{He}$ - $^4\text{He}$  LM2M2 interaction and find good agreement. We furthermore show that in this effective field theory approach no three-body force is required at leading order and that *universal* van der Waals physics leads to a universal correlation between three-body observables in the absence of an Efimov three-body parameter.

---

\* [dodell@ohio.edu](mailto:dodell@ohio.edu)

† [lplatter@utk.edu](mailto:lplatter@utk.edu)

## I. INTRODUCTION

Effective field theories (EFT) have led to significant advances in the fields of nuclear and particle physics [1, 2]. In atomic physics, EFTs have been successfully applied to systems of ultracold atoms with large scattering length that also display the so-called Efimov effect [3, 4]. At leading order (LO) in this large-scattering-length and short-range EFT (SR-EFT), the resulting scattering equations are the same as the ones arising from zero-range interactions [5]. Therefore, a three-body parameter and thereby one experimental three-body datum is required to make predictions within this framework [3, 6]. Generally, EFTs are low-energy expansions that exploit a separation of scales (e.g. between large scattering length and range of the interaction) as an expansion parameter. This implies that every EFT calculation has an intrinsic uncertainty arising from the truncation of the expansion which is highly useful for the comparison with experimental data.

Recently, it was observed that the Efimov three-body parameter in atomic systems can be derived from the coefficient of the van der Waals tail of the atom-atom interaction. A number of theoretical works used various models with long-range van der Waals tails to study these observations and found that the two-body van der Waals interaction alone can indeed predict the three-body observables of ultracold gases with a large scattering length accurately (see Ref. [7] for a recent review, a discussion of the origin of the so-called van der Waals universality and a more complete list of references). However, a recent study [8] has also demonstrated that there are some caveats to universality that are related to the details of the atom-atom interaction. These findings immediately raise the questions whether the van der Waals potential can be the starting point for atoms whose interaction contains the van der Waals tail and also what would be the expected uncertainty of a leading order calculation within such a framework. Van der Waals universality implies in particular the existence of a short-distance length scale smaller than  $\beta_6$ , the length scale associated with the van der Waals interaction. The size of this short-distance length scale is not immediately clear, however, it could be determined once certain aspects of the low-energy expansion have been established.

We note that some effort has already been made to understand (i) the properties of a two-body system interacting solely through a van der Waals interaction [9] and (ii) the contributions that need to be included beyond leading order [10, 11]. However, in this

manuscript, we will focus on the  $^4\text{He}$  three-body system that also displays a large two-body scattering length and try to answer whether a simple van der Waals potential can be the starting point for an effective theory description of atomic three-body systems. To answer this question, one must confront three related questions: Does the proposed leading order of this new EFT lead to meaningful results that one can hope to systematically improve upon? What is the low-energy EFT expansion parameter and thereby the uncertainty of a leading-order calculation? And finally, what are the required physical parameters that will enter the higher order calculations?

As a starting point, we will consider the system of three  $^4\text{He}$  atoms. The  $^4\text{He}$  interaction leads to a large scattering length and various potential models have been constructed to reproduce these features. In the three-body system there are two three-body bound states: a shallow one, often considered to be an Efimov state associated with the large scattering length, and a deep state that is considerably impacted by effective-range corrections. These three-body observables were calculated many times with the afore-mentioned potentials, and in particular the so-called LM2M2 model was used in several theoretical studies[12–15]. We will therefore use it as a template for our microscopic underlying theory which serves as the basis of our EFT approach. This means that selected LM2M2 results for observables will be taken to constrain our van der Waals EFT model while others are expected to be reproduced by the van der Waals EFT with an uncertainty related to its inherent expansion parameter.

Finally, we should note that this system has also received renewed attention because a detection of the excited (so-called Efimov) three-body state was achieved [16].

This manuscript is arranged as follows. In Sec. II, we present the relevant potential, the analytical predictions by Gao in the two-body sector, the specifics of our implementation, and some relevant details of the LM2M2 potential. In Sec, III, we will discuss the details of our renormalization scheme and the low-energy results obtained in the two-body sector. Section IV contains our results in the three-body sector and insights into correlations between the scattering and bound-state regions. The results are obtained by solving the corresponding equations in the momentum-space partial-wave representation; the details can be found in Ref. [17] and therefore are not discussed here. Finally, we summarize our work, draw conclusions, and discuss further advancements in Sec. V.

## II. THE VAN DER WAALS INTERACTION

### A. Previous Work

In this work, we will consider an interaction that at long distances has an attractive van der Waals tail of the form

$$V(r) = -\frac{C_6}{r^6}. \quad (1)$$

The van der Waals *strength*  $C_6$  can be converted into a *characteristic* length scale  $\beta_6 \equiv (mC_6)^{1/4}$ , where  $m$  is the mass of the interacting particles. Gao derived solutions to the attractive  $1/r^6$  potential in Ref. [9]. The bound state wave function of the state with energy  $E$  in partial wave  $l$  is written as a linear combination of two solutions,  $f_{El}(r)$  and  $g_{El}(r)$  of the van der Waals interaction

$$u_{El}(r) = A_{El} [f_{El}(r) - K_l g_{El}(r)] , \quad (2)$$

where  $A_{El}$  is a normalization coefficient and  $K_l$  denotes the so-called short-range  $K$ -matrix that fixes here an additional boundary condition on the wave function that is required due to the potentials singularity at the origin. The precise forms of the functions  $f_{El}(r)$  and  $g_{El}(r)$  are given in Ref. [9]. For bound states, their asymptotic form is given by

$$\begin{aligned} f_{El}(r) &\rightarrow (2\pi\kappa)^{-1/2}(W_{f-}e^{\kappa r} + W_{f+}e^{-\kappa r}) , \\ g_{El}(r) &\rightarrow (2\pi\kappa)^{-1/2}(W_{g-}e^{\kappa r} + W_{g+}e^{-\kappa r}) , \end{aligned} \quad (3)$$

where  $\kappa$  represents the bound state momentum and the coefficients  $W_{f\pm, g\pm}$  depend on the energy  $E$  and the angular momentum  $l$  of the of bound state [9].

Requiring Eq. (2) to give normalizable solution implies that the terms proportional to  $e^{\kappa r}$  in Eq. (3) cancel and leads to

$$K_l(E) = \chi_l(\Delta) = W_{f-}/W_{g-} , \quad (4)$$

where  $\Delta = 2\mu E\beta_6^2/(16\hbar^2)$ .

The solid line in Fig. 1 shows the function  $\chi_{l=0}(\Delta)$  for the  $\beta_6$  value associated with the  ${}^4\text{He}-{}^4\text{He}$  interaction. The intersections between the dashed line and the solid line give the two-body binding energies in terms of the rescaled energy variable  $\Delta$  once the boundary condition is chosen either by adjusting the energy ( $\Delta$ ) - position of one the intersections or by adjusting a scattering observable.

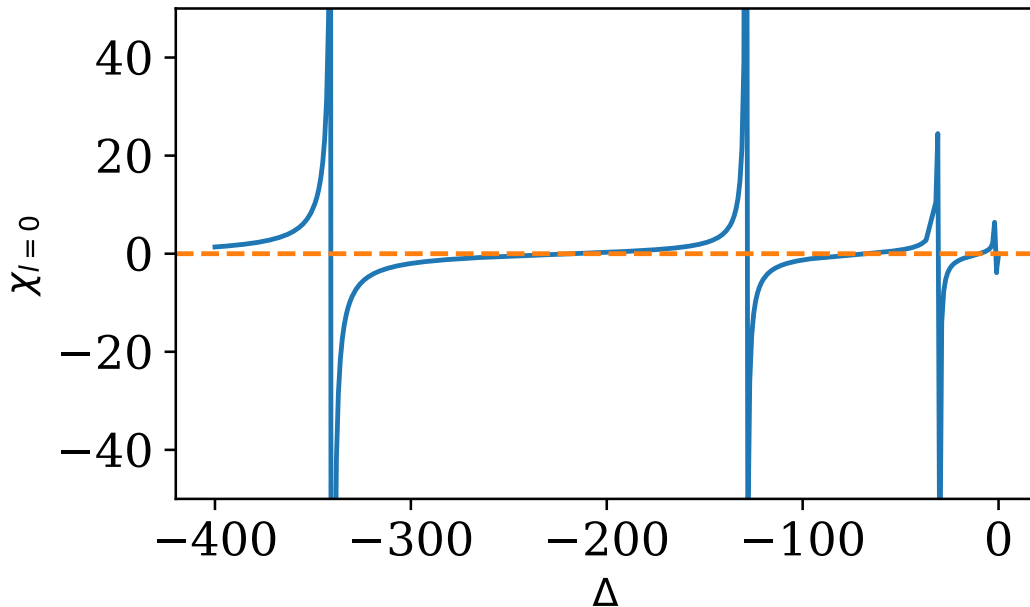


Figure 1.  $\chi_{l=0}$  as a function of the dimensionless parameter  $\Delta$ . The solid, blue line is  $\chi_{l=0}$ . The dashed, orange line is the value of  $\chi_{l=0}$  at the  ${}^4\text{He}_2$  binding energy.

Expressions for the asymptotic solutions at positive energies can be used to derive expressions for the two-body  $t$ -matrix and thereby for the effective range parameters. Gao obtains for the S-wave scattering length and effective range [18]

$$\begin{aligned}
 a_s &= \frac{2\pi}{[\Gamma(1/4)]^2} \frac{K_0(0) - 1}{K_0(0)} \beta_6, \\
 r_s &\approx \frac{[\Gamma(1/4)]^2}{3\pi} \frac{K_0(0)^2 + 1}{[K_0(0) - 1]^2} \beta_6,
 \end{aligned}
 \tag{5}$$

where the  $K_0(0)$  is evaluated at zero energy (threshold). The relation for  $r_0$  is truncated under the assumption that the derivative of the short-range  $K$ -matrix is small. In effect, we can calculate the boundary condition,  $K_0(0)$ , from  $a_s$ , and then calculate  $r_s$ .

The scattering length is then dependent on the van der Waals length scale,  $\beta_6$ , and the short-range  $K$ -matrix,  $K_l$ , evaluated in the  $S$ -wave channel at zero energy.

## B. Numerical implementation

As a LO approximation of the  ${}^4\text{He}$  system, we take the  $C_6$  coefficient from the LM2M2 potential [19], and account for the short-distance behavior with a single, two-body, momentum-

space counterterm described below. We regulate (cut off) the local part of the potential at distances well below  $R$  with a regulator function  $\rho(r; R)$

$$\rho(r; R) = \left[1 - e^{-(10r/R)^2}\right]^8, \quad (6)$$

such that the full coordinate-space potential is

$$V(r) \equiv \rho(r; R)V_6(r). \quad (7)$$

The local regulator is effective at a distance  $R/10$  that is considerably shorter compared to the nonlocal regulators described below. This ensures that cutoff effects are isolated to a single scale — that there are no interferences between the local and nonlocal regulators in the momentum-space potential. It is also worthwhile noting that other regulators can be used but that their specific form can influence the rate of convergence with respect to the number of grid points in numerical calculations.

We will solve for two- and three-body observables in momentum space. We therefore calculate the momentum space interaction as a regulated Fourier transform of the regulated coordinate space version of the van der Waals interaction

$$\tilde{V}_{l,l'}(p, p') = \tilde{\rho}(p; R)\tilde{\rho}(p'; R) \frac{2}{\pi} \int_0^\infty dr r^2 j_l(pr)V(r)j_{l'}(p'r), \quad (8)$$

where

$$\tilde{\rho}(p; R) = e^{-(pR/2)^8}, \quad (9)$$

is the nonlocal regulator and  $j_l(pr)$  are the spherical Bessel functions.

Once regulated at a short distance,  $R$ , physical observables acquire dependence on the arbitrary choice of  $R$  which is removed by the introduction of the counterterm

$$\tilde{\chi}_{l,l'}(p, p'; R) = g_l(R) p^l (p')^{l'} \tilde{\rho}(p; R)\tilde{\rho}(p'; R) \delta_{l,l'}. \quad (10)$$

For every value of  $R$  the counterterm  $g_l(R)$  is readjusted such that the chosen two-body observable is reproduced. We will refer to the functional dependence of  $g_l(R)$  as renormalization group (RG) flow. A more detailed discussion of the renormalization scheme can be found in Subsection III A. Similarly, a more detailed discussion of the calculation of two- and three-body observables can be found in [17].

### C. Details of the LM2M2 Potential

The LM2M2 potential is one of several potentials developed for the interaction of  $^4\text{He}$  atoms [19]. We will use it here because of a large number of few-body calculations that have been carried out with this interaction. This potential is a sum of  $r^{-6}$ ,  $r^{-8}$ , and  $r^{-10}$  terms, each having a separate strength coefficient. We can quantify how *pure* the van der Waals tail is in the LM2M2 interaction by converting these coefficients  $C_6$ ,  $C_8$  and  $C_{10}$  into corresponding length scales. In Tbl. I, we show the length scales associated with each inverse-power-law contribution to the LM2M2 potential. We can see that the van der Waals tail has the largest length scale. We expect therefore the features of the trimer states to be dominated by the van der Waals interaction.

A conservative estimate of the LO theory's uncertainties can be formulated from the energy scales given in Tbl. I. The ground-state trimer with 126.4 mK binding energy is the observable farthest from threshold that we calculate. The ratio of the binding energy to the energy scale associated with  $\beta_8$ , the lowest breakdown scale of the  $^4\text{He} - ^4\text{He}$  interaction, is approximately 1/9. Therefore the ratio of momentum scales is approximately 1/3. We use this ratio to conservatively estimate our LO theory uncertainty at 30%.

In addition, there are three other terms in the LM2M2 potential. The first is a multiplicative regulator function of the form

$$F(x) = \begin{cases} e^{-(D/x-1)^2} & x \leq D \\ 1 & x \geq D \end{cases} \quad (11)$$

where  $x = r/r_m$  and  $r_m = 2.9695 \text{ \AA}$ . For the LM2M2,  $D = 4.2 \text{ \AA}$ . However, due to the functional form of  $F(x)$ , the value of  $F(x)$  does not drop below 0.5 until  $r < 2.5 \text{ \AA}$ . Therefore, we conclude that the range of the regulator function is comparable to  $\beta_{10}$  which is significantly smaller than the scale of interest,  $\beta_6$ .

The second remaining term in the LM2M2 potential is the short-distance repulsion, which is effectively a Gaussian centered at approximately  $-8.3 \text{ \AA}$  with a  $1\text{-}\sigma$  width of  $1.5 \text{ \AA}$ . Of course, in the relevant region,  $r > 0$ , this Gaussian function overcomes the divergences of the inverse-power-law terms. A conservative estimate for the range of the short-distance repulsion is the minimum of the total potential, which occurs below  $3 \text{ \AA}$ , well below  $\beta_6$ .

The final term to be addressed is a sine function defined in Eq. (A3) in Ref. [19]. Its peak

$n$	$\beta_n$	$(m\beta_n^2)^{-1}$ [mK]
6	5.38	419.18
8	3.62	923.42
10	3.09	1272.3

Table I. The length scales  $\beta_6$ ,  $\beta_8$ , and  $\beta_{10}$  and the corresponding energy scales arising from the different contributions to the LM2M2 potential

value is small enough relative to the other terms in the potential, therefore its contribution is insignificant. To relieve any residual concerns, we point out that the peak of this term occurs at  $3.65 \text{ \AA}$ , which is comparable to  $\beta_8$ , but again, we emphasize that the magnitude at this peak is relatively small.

### III. THE $^4\text{HE}$ TWO-BODY SYSTEM

#### A. Renormalization Scheme

We tune the counterterm in Eq. (10) in each two-body partial wave to reproduce arbitrarily chosen low-energy observable(s). In the  $S$ -wave channel,  $g_0(R)$  is tuned to yield a shallow two-body bound state with the binding energy  $B_2 = 1.31 \text{ mK}$ . In the  $D$ -wave channel  $g_2(R)$  is tuned to reproduce the two-body phase shift at  $E = 67\text{mK}$  ( $\Delta = 0.01$ ) found using the LM2M2 potential. Finally, the  $G$ -wave counterterm  $g_4(R)$  is tuned to fit the LM2M2 phase shifts below  $15\text{K}$ . The upper energy limit of the  $G$ -wave phase shifts was chosen to avoid low-lying resonances. The  $l = 4$  centrifugal barrier of the local van der Waals interaction constructed here peaks between  $14$  and  $15 \text{ K}$ . Forcing our system to reproduce the LM2M2  $G$ -wave phase shifts over this large region successfully prevents resonances, otherwise rapidly moving with  $R$ , from interfering with low-energy three-body observables.

This procedure generates a RG *flow*, a function that gives the counterterm coupling strength's dependence on the short-distance regulator scale,  $R$ , that is shown for  $S$ -,  $D$ -, and  $G$ -waves in Fig. 2.



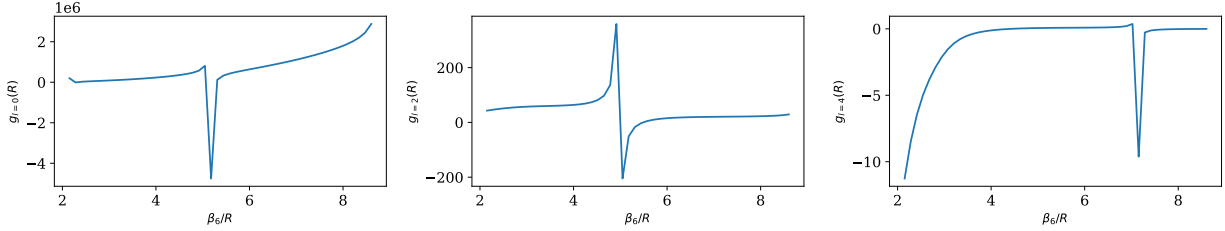


Figure 2. The strengths of the counterterms  $g_0(R)$ ,  $g_2(R)$ , and  $g_4(R)$  as functions of the dimensionless parameter  $\beta_6/R$ . The units of  $g_l(R)$  are  $\text{K}\cdot\text{\AA}^{2l+3}$ .

## B. Two-Body Results

To demonstrate the effectiveness of our LO potential to capture the relevant physical behavior of the  ${}^4\text{He} - {}^4\text{He}$  interaction, we show in Fig. 3 the cutoff dependence of the S-wave scattering length  $a_s$  (left panel) and effective range  $r_s$  (right panel), respectively. The error bands are generated by the covariance estimates from a non-linear, least-squares fit. The LM2M2 results for these parameters are  $a_s = 100.2 \text{ \AA}$  and  $r_s = 7.33 \text{ \AA}$  and are included in both plots to establish the degree to which the  ${}^4\text{He} - {}^4\text{He}$  interaction at low energies is characterized by the van der Waals tail.

In an EFT, we expect the convergence of observables to follow  $\mathcal{O}(1/R) = \mathcal{O}_0 [1 + \sum_{n=1}^{\infty} c_n (qR)^n]$ . As shown in [17], this simple expansion is not always observed in practice. Oscillatory functions and non-integer powers of  $qR$  can obscure the analytical description of cutoff dependence — even at small values of  $R$ . In [17], the analysis was conducted for the attractive  $1/r^3$  potential. Here, while similar features can be seen in the figures below, a stronger singularity makes the calculations much more difficult numerically, rendering the analysis of the logarithmic derivative inconclusive. Therefore, asymptotic estimates provided in the following results are based on qualitative analyses of the short-distance cutoff dependencies.

Figure 3 shows the convergence of  $a_s$  and  $r_s$  with respect to the dimensionless variable  $\beta_6/R$ . The quantities are fit according to the modified effective range expansion derived by Gao [18],

$$k \cot \delta_0 = -\frac{1}{a_s} + \frac{r_s}{2} k^2 + c_3 k^3 + c_4 k^4 + \mathcal{O}(k^4 \ln k). \quad (12)$$

Estimated values for  $a_s$  and  $r_s$  in the  $\beta_6/R \rightarrow \infty$  limit are given in Table IV B. In comparison to the LM2M2 results,  $a_s$  is within 0.5% and  $r_s$  within 2%. The relative difference between

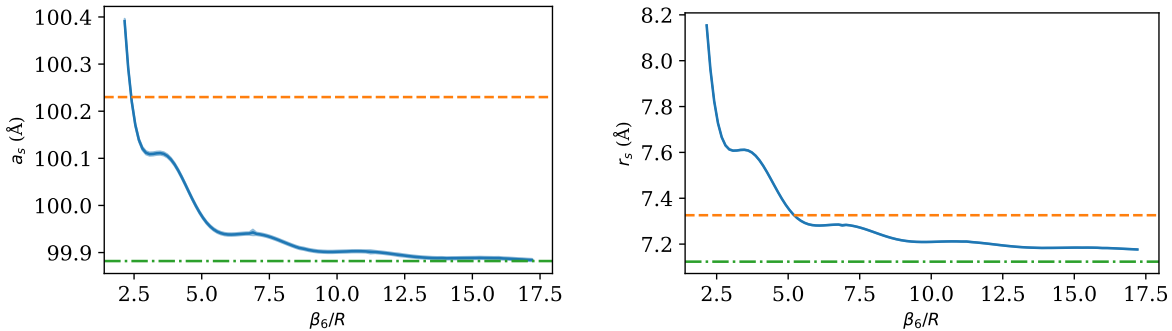


Figure 3. The  ${}^4\text{He}$  two-body scattering length (left panel) and the effective range (right panel) as functions of  $\beta_6/R$ . The solid blue lines display the results obtained with the renormalized van der Waals potential, the shaded blue band gives the numerical uncertainty for  $a_s$ . The orange dashed lines represent the respective results obtained with the LM2M2 potential, while the green dot-dashed lines show Gao’s prediction based on Eq. 5.

$a_s$  and the Gao prediction is on the order of  $10^{-5}$ . The effective range differs by less than a percent. The scattering length is given *for free* in that universality, of the generic kind, guarantees this result. The agreement of  $r_s$  with the LM2M2 and Gao’s prediction [18] is the result of van der Waals universality.

The agreement between our results and Gao’s predictions is noticeably better for  $a_s$  than for  $r_s$ . We point out a few caveats associated with this observation. First,  $r_s$  can be sensitive to the energy range included in the fit to Eq. (12), an arbitrary choice. Similarly, that fit is also sensitive to the number of terms treated in Eq. (12). Finally, the analytical prediction in [9] for  $r_s$  includes a term proportional to the energy derivative of the  $K$ -matrix at zero energy. This term is assumed to be small and therefore not included in the evaluation here.

As a further demonstration of the agreement between our results and the Gao predictions, we show the two-body spectrum in Fig. 4. As  $\beta_6/R$  increases, the degree to which the van der Waals tail dominates the long-range behavior increases, moving our results towards those predicted by Gao. Indeed, the binding energies of deeper two-body states are approaching the Gao’s predictions — precisely the behavior we expect.

Furthermore, Gao predicts that for higher partial waves,

$$\tan \delta_{l \geq 2} = \frac{3\pi}{32(l+1/2)[(l+1/2)^2-4][(l+1/2)^2-1]}(k\beta_6)^4. \quad (13)$$

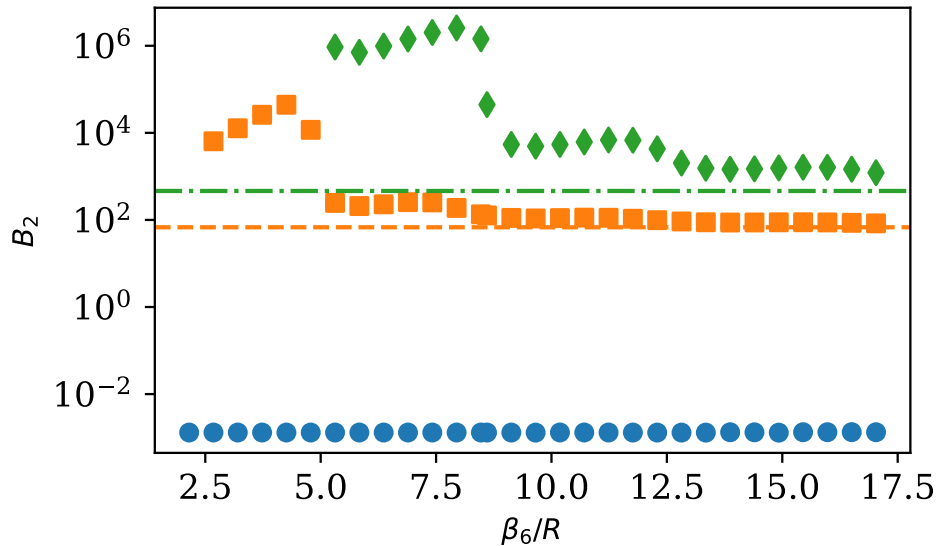


Figure 4. Evolutions of the two-body s-wave spectrum with a decreasing short-distance cutoff  $R$ . The shallowest state (blue circles) is fixed and shown together with the next two states in the spectrum. The first one (orange squares) is compared to the Gao prediction for the next deeper state (dashed, orange lines). The second one (green diamonds) is similarly compared to the Gao prediction (green, dash-dotted line). Predictions are discussed in II A.

In the left panel of Fig. 5 we compare the  $D$ -wave phase shifts of our pure van der Waals interaction with the result obtained using the LM2M2 potential and the Gao prediction [18]. The different lines shown correspond to different values of the short-distance regulator  $R$ . The results agree very well at low momenta while they start to deviate at larger momenta. However, we note that the scale on which the phaseshift is shown is relatively small. A relative comparison is shown in the right panel of Fig. 5 where the differences between small values of  $\tan \delta$  are highlighted. The van der Waals system, as expected, consistently stays closer to the predicted behavior whereas the LM2M2 results quickly deviate presumably due to significant contributions from terms in the potential dominating at the short distances being probed at higher energies.

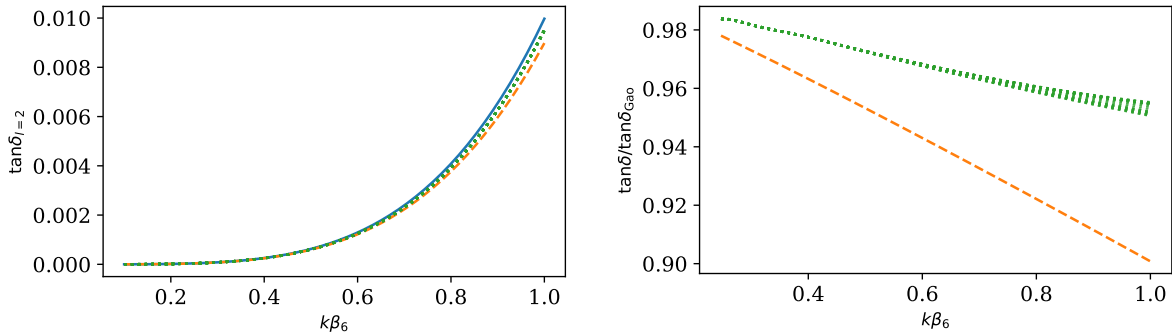


Figure 5. [Left panel] The van der Waals (green, dotted lines) and LM2M2 (orange, dashed line)  $d$ -wave phase shifts, given in terms of  $\tan \delta$ , are compared to Gao's predictions (blue, solid line). The different overlapping van der Waals lines correspond to different values of  $R$ . [Right panel] The ratio of  $\tan \delta_{l=2}$  to the prediction by Gao as a function of  $k\beta_6$ . Where applicable, the colors and linestyles are as in the left panel.

#### IV. THE ${}^4\text{He}$ THREE-BODY SYSTEM

We will now calculate three-body observables using the van der Waals interaction tuned to reproduce  ${}^4\text{He}$  two-body parameters. We emphasize that the theory developed at this order is uninformed by  ${}^4\text{He}_3$  observables which is a very different starting point in comparison to the SR-EFT.

##### A. Binding energies

We first calculate the ground state binding energy of the  ${}^4\text{He}$  trimer. The LM2M2 potential prediction for this state is 126.4 mK [15]. In Fig. 6 we show the binding energy of the trimer ground state as a function of the dimensionless parameter  $\beta_6/R$ . The blue circles give the results when only  $S$ -wave two-body interaction is included in the calculation, orange squares include also the  $D$ -wave, and green diamonds include  $G$ -wave as well. Since  $\beta_6$  is the characteristic length scale of the van der Waals interaction, we expect that only values of  $\beta_6/R > 1$  capture the important features of the van der Waals interaction. As indicated by the figure, in the  $\beta_6/R \rightarrow \infty$  and  $l_{\text{max}} \rightarrow \infty$  limits, a converged value near (within 10%) the LM2M2 result is obtained.

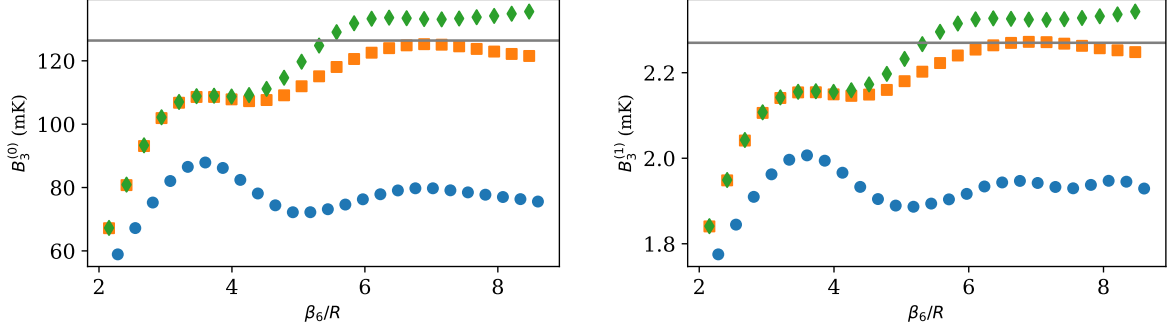


Figure 6. Three-body binding energies for the ground (left) and excited (right) states as functions of  $\beta_6/R$ . The blue circles are the calculated energies using  $S$ -wave only. Orange squares include  $D$ -wave in addition, and green diamonds include also  $G$ -wave.

The LM2M2 potential leads to a binding energy of 2.27 mK for the excited trimer state [15]. From an energy-scale point of view, the excited state appears to be a better observable to study for the purposes of EFTs: For the SR-EFT, it is a state whose binding energy is close to the energy scale of the two-body bound state and that is thereby clearly within the range of convergence of this EFT. For our van der Waals EFT it is well separated from the energy scales associated with  $\beta_8$  and  $\beta_{10}$  shown in Table I. The regulator dependence of the excited state is shown in the right panel of Fig. 6. The convergence toward the LM2M2 result is similar to that of the ground-state trimer and further demonstrates the accuracy of describing the  ${}^4\text{He} - {}^4\text{He}$  interaction with a van der Waals EFT.

Estimates for the three-body binding energies in the  $\beta_6/R \rightarrow \infty$  limit are given in Table IV B. Contributions from partial waves where  $l > 4$  are neglected. Based on the rapid decrease in the contribution to  $B_3^{(n)}$  going from  $l_{\max} = 2$  to  $l_{\max} = 4$ , we expect higher partial waves to have even less of an impact. This effect has already been observed in [20] for the LM2M2 potential.

## B. Atom-dimer scattering

The atom-dimer scattering properties of the  ${}^4\text{He}$  have been considered previously with various realistic atom-atom interactions. In Ref. [15], a value of 115.22 Å is obtained for the LM2M2 potential. In Fig. 7, we show the convergence of the atom-dimer scattering length

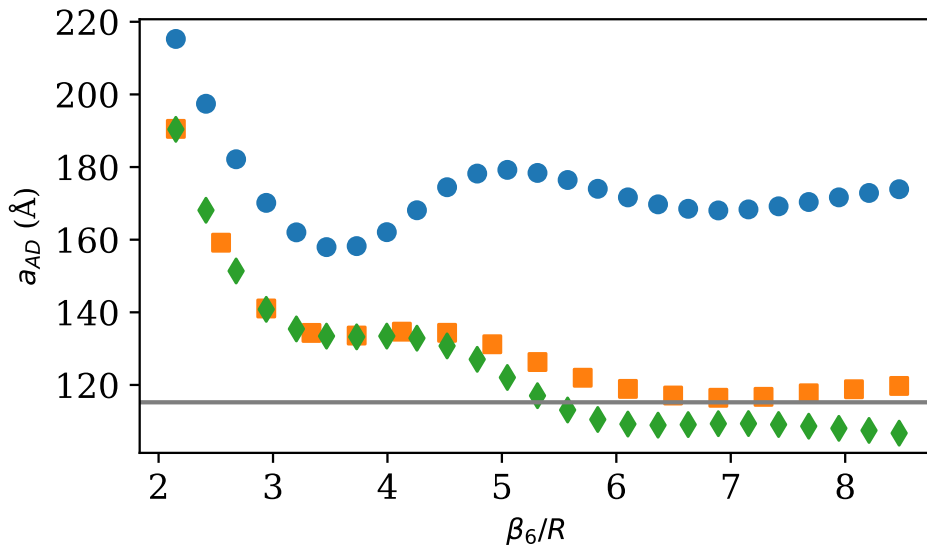


Figure 7. Atom-dimer scattering length  $a_{AD}$  as a function of  $\beta_6/R$ . The horizontal solid line gives the result of Ref. [15]. Symbols and colors are as in Figure 6

with respect to  $\beta_6/R$ . Symbols and colors are as they appear in Fig. 6. We observe again that at least  $S$ - and  $D$ -waves have to be included to obtain good agreement with the results of the LM2M2 potential. Assuming again that the regulator dependence scales as  $\beta_6/R$ , we determine the atom-dimer scattering length to be  $105 \pm 10$  Å in the limit of  $\beta_6/R \rightarrow \infty$ . Though not shown in the figure, we obtained stable numerical results for  $S$ - and  $D$ -wave calculations of  $a_{AD}$  for values of  $\beta_6/R \lesssim 17$  and verified that the convergence is stable.

We have also calculated the atom-dimer effective range and find  $r_{AD} = 85 \pm 10$  Å but note that the extraction of this observable is difficult due to its strong regulator dependence. This result has to be compared to the LM2M2 result of 79.0 Å given in Ref. [21]. The convergence of  $B_3^{(0)}$ ,  $B_3^{(1)}$ , and  $a_{AD}$  with respect to the  $\beta_6/R \rightarrow \infty$  limit indicates that a three-body force is not required at LO to obtain renormalized results.

### C. Universal correlations and a comparison to the short-range EFT

A correlation between the neutron-deuteron scattering length and the triton binding energy was observed in calculations with phaseshift equivalent interactions and is known as the Phillips line [22]. In the EFT with contact interactions, this correlation can easily be

$\mathcal{O}$	$\mathcal{O}((\beta_6/R)_{\max})$	$\delta\mathcal{O}$
$a_s$ ( $\text{\AA}$ )	99.9	0.1
$r_s$ ( $\text{\AA}$ )	7.2	0.1
$B_3^{(0)}$ (mK)	135	10
$B_3^{(1)}$ (mK)	2.3	0.1
$a_{AD}$ ( $\text{\AA}$ )	105	10
$r_{AD}$ ( $\text{\AA}$ )	85	10

Table II. Estimates for various observables ( $\mathcal{O}$ ) and conservative estimates of their associated uncertainties ( $\delta\mathcal{O}$ ) based on the convergence behavior shown in the previous figures.

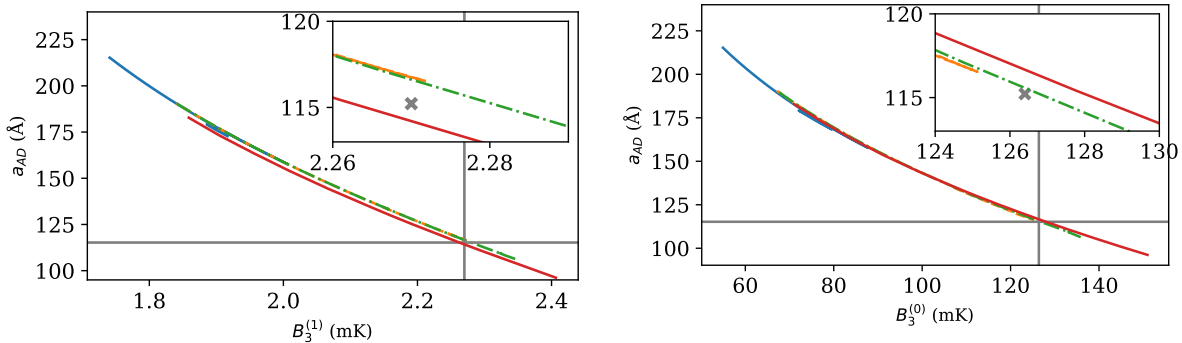


Figure 8. Left panel: The correlation between the excited state binding energy  $B_3^{(1)}$  and the atom-dimer scattering length  $a_{AD}$ . Right panel: The correlation between the trimer ground state energy and the atom-dimer scattering length  $a_{AD}$ . [Both panels]  $S$ -wave only results are shown as a blue, solid line. Results including  $D$ - and  $G$ -waves are shown as orange, dashed and green, dot-dashed lines, respectively. The red, solid line is the prediction from SR-EFT.

reproduced by varying the three-body parameter [23]. Reference [24] used the SR-EFT to analyze universal aspects of this system and displayed the Phillips line for the  $^4\text{He}$  system produced at LO. In Refs. [25, 26], SR-EFT calculations were carried out at next-to-leading order (NLO) and next-to-next-to-leading order (N2LO) for the  $^4\text{He}$  system by including the effects of a finite effective range and it was found that the convergence behavior of the EFT expansion is poor for the ground state.

In Fig. 8, we display the correlation between  $a_{AD}$  and both  $B_3^{(1)}$  and  $B_3^{(0)}$  values obtained

by changing the regulator  $R$ . The results show an approximately linear correlation. However, more importantly: results that were obtained with different numbers of included partial wave channels fall on nearly the same correlation line. In addition to our own results, we include the results corresponding to the values reported in [15] shown as grey horizontal and vertical lines. The intersection of the lines representing those results falls in excellent agreement with our own calculations. In Fig. 8, we show the so-called Phillips line predicted by SR-EFT as a red, solid line. The agreement with this Phillips line traced out by our calculations is quite good. For the excited state, the differences between the predicted correlations and the results of [15] are qualitatively the same. In the case of the ground state, the correlation from van der Waals EFT is noticeably closer to intersection of the results reported in [15]. It is particularly remarkable that the results for calculations that include different numbers of partial waves in the two-body subsystem lie on the same line. The reason for this is that the low-energy scattering features of higher partial waves are not relevant to obtain the correlations between observables in the  $^4\text{He}$  three-body sector. At distances where the van der Waals interaction dominates the centrifugal barrier the short-range attraction is the same in all partial waves. The degree to which this attraction is exposed determines the location on the  $^4\text{He}$  Phillips line.

## V. SUMMARY

In this work, we considered the three-body system composed of  $^4\text{He}$  atoms as a starting point for a description of few-body observables with an EFT whose leading order is the long-range van der Waals interaction. We analyzed for the first time the dependence of three-body observables on the short-distance regulator employed in calculations with the van der Waals potentials. Our numerical results converge and become independent of the short-distance regulator which leads to the conclusion that no three-body force is required when the van der Waals interaction with a two-body counterterm is considered to be the LO of an EFT. We provided values with uncertainty estimates for the trimer binding energies and for the atom-dimer scattering length in the limit of zero short-distance regulator.

We demonstrated also that this leading order calculation provides a good description of the  $^4\text{He}$  trimer system, *i.e.*, the binding energies of the two trimer bound states and the atom-dimer scattering length are very close to the results obtained with the LM2M2 potential. In



agreement with previous calculations using  $^4\text{He}$  potentials, we observe that higher two-body partial waves have an important impact (specifically the  $l = 2$  contribution) on the three-body observables but that the size of their contribution decreases rapidly with increasing  $l$ . Also, comparing the result for the deep trimer state obtained in SR-EFT and van der Waals EFT indicates that the latter apparently contains important finite range contributions as the result is significantly closer to the potential result. This is encouraging as higher-order calculations with the SR-EFT indicate that the deep trimer state is outside of the radius of convergence of the SR-EFT [26]. We furthermore found that the inclusion of higher partial waves does not shift significantly the so-called Phillips line, the correlation between the atom-dimer scattering length and three-body binding energy obtained by varying the short-distance regulator, but rather move along the Phillips line.

Two important developments should be carried out in the near future. First, the structure and impact of higher order corrections needs to be analyzed. As a first step, momentum-dependent contact interactions can be introduced in the S-wave channel. It would then be necessary to determine the observables to fit this additional low-energy parameter to, e.g. low-energy phaseshifts in a certain energy range. Developments related to the use of the so-called modified effective range expansion in the context of EFTs [27] and recently developed prescriptions for the construction of ordering schemes for singular interactions [28] make this avenue particularly promising. Second, this approach should be used to analyze the three-body spectrum for a variable scattering length, *i.e.*, for systems close to a Feshbach resonance. This will provide further insights on the uncertainties for three-body observables and universal relations established for the van der Waals universality.

## ACKNOWLEDGMENTS

We thank H.-W. Hammer, D. R. Phillips, and S. König for useful discussions. This work has been supported by the National Science Foundation under Grant No. PHY-1555030, the Office of Nuclear Physics, U.S. Department of Energy under Contract No. DE-AC05-00OR22725, and the National Nuclear Security Administration No. DE-NA0003883. This work used the Extreme Science and Engineering Discovery Environment (XSEDE), which is supported by National Science Foundation grant number ACI-1548562, allocation number

- [1] H.-W. Hammer, S. König, and U. van Kolck, *Rev. Mod. Phys.* **92**, 025004 (2020), 1906.12122.
- [2] A. V. Manohar (2018), 1804.05863.
- [3] V. Efimov, *Phys. Lett.* **33B**, 563 (1970).
- [4] E. Braaten and H. W. Hammer, *Phys. Rept.* **428**, 259 (2006), cond-mat/0410417.
- [5] G. Skorniakov and K. Ter-Martirosian, *Sov. Phys. JETP* **4**, 648 (1957).
- [6] P. F. Bedaque, H. Hammer, and U. van Kolck, *Nucl. Phys. A* **646**, 444 (1999), nucl-th/9811046.
- [7] P. Naidon and S. Endo, *Reports on Progress in Physics* **80**, 056001 (2017), URL <https://doi.org/10.1088/1361-6633/aa50e8>.
- [8] R. Chapurin, X. Xie, M. J. Van de Graaff, J. S. Popowski, J. P. D’Incao, P. S. Julienne, J. Ye, and E. A. Cornell, *Phys. Rev. Lett.* **123**, 233402 (2019), URL <https://link.aps.org/doi/10.1103/PhysRevLett.123.233402>.
- [9] B. Gao, *Phys. Rev. A* **58**, 1728 (1998), URL <https://link.aps.org/doi/10.1103/PhysRevA.58.1728>.
- [10] B. R. Holstein, *Phys. Rev. D* **78**, 013001 (2008), URL <https://link.aps.org/doi/10.1103/PhysRevD.78.013001>.
- [11] N. Brambilla, V. Shtabovenko, J. Tarrús Castellà, and A. Vairo, *Phys. Rev. D* **95**, 116004 (2017), 1704.03476.
- [12] E. A. Kolganova, A. K. Motovilov, and W. Sandhas, *Phys. Rev. A* **70**, 052711 (2004), URL <https://link.aps.org/doi/10.1103/PhysRevA.70.052711>.
- [13] A. K. Motovilov, W. Sandhas, S. A. Sofianos, and E. A. Kolganova, *Eur. Phys. J. D* **13**, 33 (2001), physics/9910016.
- [14] D. Blume and C. H. Greene, *The Journal of Chemical Physics* **112**, 8053 (2000), <https://doi.org/10.1063/1.481404>, URL <https://doi.org/10.1063/1.481404>.
- [15] V. Roudnev and M. Cavagnero, *Journal of Physics B: Atomic, Molecular and Optical Physics* **45**, 025101 (2011), URL <https://doi.org/10.1088/0953-4075/45/2/025101>.
- [16] M. Kunitski, S. Zeller, J. Voigtsberger, A. Kalinin, L. P. H. Schmidt, M. Schoffler, A. Czasch, W. Schollkopf, R. E. Grisenti, T. Jahnke, et al., *Science* **348**, 551–555 (2015), ISSN 1095-9203,

URL <http://dx.doi.org/10.1126/science.aaa5601>.

- [17] D. Odell, A. Deltuva, J. Bonilla, and L. Platter, *Phys. Rev. C* **100**, 054001 (2019), 1903.00034.
- [18] B. Gao, *Phys. Rev. A* **58**, 4222 (1998), URL <https://link.aps.org/doi/10.1103/PhysRevA.58.4222>.
- [19] R. A. Aziz and M. J. Slaman, *The Journal of Chemical Physics* **94**, 8047 (1991), <https://doi.org/10.1063/1.460139>, URL <https://doi.org/10.1063/1.460139>.
- [20] A. Deltuva, *Few-Body Systems* **56**, 897–903 (2015), ISSN 1432-5411, URL <http://dx.doi.org/10.1007/s00601-015-1006-8>.
- [21] R. Lazauskas and J. Carbonell, *Physical Review A* **73** (2006), ISSN 1094-1622, URL <http://dx.doi.org/10.1103/PhysRevA.73.062717>.
- [22] A. C. Phillips, *Nucl. Phys. A* **107**, 209 (1968).
- [23] P. F. Bedaque, H. Hammer, and U. van Kolck, *Phys. Rev. Lett.* **82**, 463 (1999), nucl-th/9809025.
- [24] E. Braaten and H. W. Hammer, *Phys. Rev. A* **67**, 042706 (2003), cond-mat/0203421.
- [25] L. Platter and D. R. Phillips, *Few Body Syst.* **40**, 35 (2006), cond-mat/0604255.
- [26] C. Ji and D. R. Phillips, *Few Body Syst.* **54**, 2317 (2013), 1212.1845.
- [27] J. V. Steele and R. J. Furnstahl, *Nucl. Phys. A* **645**, 439 (1999), nucl-th/9808022.
- [28] B. Long and U. van Kolck, *Annals Phys.* **323**, 1304 (2008), 0707.4325.
- [29] J. Towns, T. Cockerill, M. Dahan, I. Foster, K. Gaither, A. Grimshaw, V. Hazlewood, S. Lathrop, D. Lifka, G. D. Peterson, et al., *Computing in Science & Engineering* **16**, 62 (2014), ISSN 1558-366X.